ANALYSIS OF ABDOMINAL FAT TISSUE IMAGES ACQUIRED WITH CONTINUOUSLY MOVING TABLE MRI

Stathis Hadjidemetriou[1]*, Ute Ludwig*[1]*, Juergen Hennig*[1]*, and Martin Buechert*[2]

[1] University Medical Center Freiburg, Department of Radiology, Medical Physics,
[2] Magnetic Resonance Development and Application Center,
60a Breisacher Street, 79106 Freiburg, Germany

ABSTRACT

The amount of visceral abdominal fat is correlated with the risk for hypertension and diabetes. In this work, an obesity study is monitored with continuously moving table whole body MRI equipped with surface coils and using the Dixon fat/water contrast and reconstruction. A method is presented for the repeatable and reliable differentiation of the imaged abdominal fat into subcutaneous and visceral. The images are first restored jointly for intensity uniformity and processed to segment the body abdominal region. Then, the exterior boundary of the visceral region separating it from the subcutaneous fat region is identified. The segmentations are performed with a combination of distance maps and graph cuts algorithms. The performance of the method has been demonstrated on data from 32 subjects.

Index Terms— MRI, Dixon reconstruction, intensity uniformity restoration, abdominal fat classification.

1. INTRODUCTION

The amount of visceral abdominal fat has been shown to correlate intimately with hypertension, hyperlipidemia, as well as the risk to develop cardiovascular disorders and diabetes [1, 2]. Effective fat quantification can be performed by imaging with CT as well as with MRI that avoids ionizing radiation. Early methods based on MRI involved the acquisition and analysis of a single or only a stack of axial slices with limited coverage restricted to only part of the abdomen [1]. More recently, a continuously moving table MRI method has been used to image the entire abdomen and even body [2, 3].

A common pre-processing step for such data has been the intensity correction. It has been performed with a variety of methods that include manual annotations [4] and the use of the ratio of fat to water intensities [5]. However, the latter method has high sensitivity to low signal to noise ratio. Intensity correction has also been performed together with the estimation of a limited number of tissue parameters provided by fuzzy c-means [1]. This does not accomodate partial volume, which is a limitation particularly for the visceral region. The segmentation has been performed with manually specified intensity thresholds followed by morphological operations [2]. Other fat segmentation methods include the fuzzy c-means method combined with active contours [1], fat classification with spatial fuzzy connectedness [6], and registration to a tissue labeled atlas [5].

In this work the abdominal fat has been imaged in high contrast with a continuously moving table whole body MRI technique and Dixon reconstruction to obtain a fat and a water image. A method is presented that allows the repeatable and reliable analysis of the imaged abdominal lipids into subcutaneous and visceral. The data is pre-processed to restore intensity uniformity [7]. It is then analyzed with the graph cuts algorithm [8] operating on distance maps to extract the abdominal body region. Then, the outer contour of the visceral region separating it from the subcutaneous fat is identified with the graph cuts algorithm operating on a simulated random walks potential [9]. The method provides the subcutaneous fat in an unsupervised manner, is able to represent the partial volume of the fat particularly in the visceral region, and is robust to noise or artifacts exterior to the body.

2. METHODS

An example axial slice with annnotations of the anatomic regions involved in this study is shown in figure 1.

2.1. Subjects and Imaging

In the context of an obesity study 32 volunteers were examined 13 men and 19 women [1]. Their average age was $48.0 \pm 6.3y$, their average weight was $99 \pm 15kg$, and their average height was $172 \pm 10.0cm$. They were examined on an 1.5Tesla scanner (Magnetom Espree, Siemens Medical Solutions, Erlangen). The scanning was performed with the subjects lying in the supine position and with a continuously moving table (CMT) double echo gradient echo sequence of flip angle $FA = 70^o$, $TE_1 = 2.38ms$, and $TE_2 = 4.76ms$.

[1]The authors would like to thank Prof. D. Koenig and Dr. P. Deibert from the Department of Sports Medicine of University Medical Center Freiburg for patient recruitment.

The FOV in the readout direction was $450mm$ and of size 320 voxels with an in-plane resolution of $1.41 \times 1.41cm^2$. The FOV in the phase direction was adapted to the size of the volunteer and varied between $240-290$ voxels, or $338-408mm$. This resulted in a matrix of variable size $320\times240-290voxels^2$. The slice thickness was $5.00cm$ without slice spacing. The body was imaged with 220 axial slices from approximately the knees to the neck. All abdominal measurements were taken in the exhaled position. A two-point Dixon reconstruction provided a water and a fat image. The abdominal region was identified manually as consisting of the axial sections between the upper hips and below the diaphragm that resulted in $54-74$ slices. The axial orientation of the body is the z axis. The dorsoventral phase encode direction is the x axis and the readout left-right direction is the y axis. The resulting abdominal fat and water images are $I_{DF}(x,y,z) \rightarrow \Re$ and $I_{DW}(x,y,z) \rightarrow \Re$, respectively.

2.2. Restoration and Foreground Extraction

The two images I_{DF} and I_{DW} are first restored jointly and non-parametrically for intensity non-uniformity. The method used is based on the joint intensity co-occurrence statistics [7]. The radius of the spatial window for the computation of the co-occurrences has been $6mm$ and the size of the Wiener deconvolution filter has been 6% of the dynamic range. The standard deviation of the spatial smoothing filter has been $45mm$. The joint intensity restoration also considers the approximately complementary signal regions of the fat and the water images. An example of reconstructed and jointly restored fat and water images is shown in figure 2. The intensity restoration is more prominent in the visceral region, but is also apparent in the subcutaneous region. The intensity restored data is smoothed with median filtering.

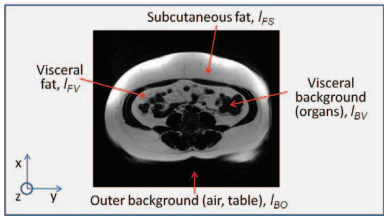


Fig. 1. An axial abdominal section with region annotations.

The joint intensity histogram of the fat and the water images is computed. The joint distribution of the background corresponding to the lack of signal in both the fat and the water images is a 2D Rayleigh distribution quantified primarily from the intensity of peak density in the joint statistics. The coordinates of the peak are equal to the standard deviations of the noise in the fat and in the water images, σ_F and σ_W, respectively. The background with no signal is set to correspond to the range $[[0, 10\sigma_F] \times [0, 10\sigma_W]]$. The back-projection of the remaining region in the statistics to image space occupies the water or fat image regions that are approximately complementary. The domain in the statistics corresponding to the signal is analyzed with a 2D expectation maximization algorithm into two distributions. One distribution corresponding to the fat signal and the other to the water signal. The spatially largest connected component in the fat image region provides the foreground fat region I_F. The connectivity preserves the abdominal region and can eliminate other regions such as the hands. The difference between I_{DF} and I_F gives the background region without signal I_B, $I_{DF} - I_F = I_B$ that corresponds to air or organs without any fat content.

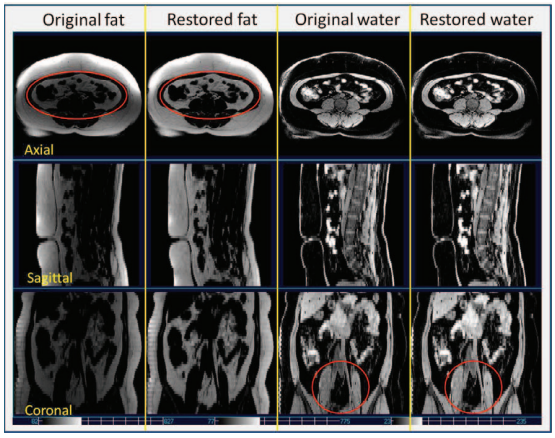


Fig. 2. Original and restored Dixon fat and water images.

2.3. Identification of the Abdominal Body Region

The first processing step uses the fat region I_F to estimate the surface enclosing the abdominal fat. This mostly coincides with the subcutaneous fat. However, the subcutaneous fat may not cover the abdominal region such as along the spinal cord and in thin subjects. The uncovered regions create bridges between interior non-fat regions and exterior air regions that are resolved with the graph cuts algorithm [8]. The seed region for the abdominal region is initially set to image I_F. These seeds are extended with a shape prior represented by a centered ellipse in every frame to give an elliptical cylinder, E_1, with a curved axis along the entire abdomen. To this end the sagittal and coronal Radon transforms (projections) are computed. The pairs of points corresponding to the 5% and 95% of the cumulative projections in each slice are used. The projection along the sagittal direction (y axis) provides $x_{0.05}$ and $x_{0.95}$, respectively. The projection along the coronal direction (x axis) provides $y_{0.05}$ and $y_{0.95}$, respectively. The points halfway between the pair in each axis $(x_{0.05} + x_{0.95})/2 = c_x$ and $(y_{0.05} + y_{0.95})/2 = c_y$, respectively, are the coordinates of the center of the ellipse, (c_x, c_y, z), for the axial slice z of I_F. The equation of the centered ellipse is $(x-c_x)^2/(1.8)^2 + (y-c_y)^2 < (6.6cm)^2$. The size of the ellipse is selected to ensure that it lies in the

interior of the abdominal fat region I_F. The extension of the seeds of the abdomen with E_1, $(I_F \vee E_1)$, limits the image domain over which the segmentation operates and results in a significant acceleration. The seed region for the background exterior to the body is a narrow frame I_M inscribed within the image boundary.

The segmentation is performed over the region remaining ambiguous between the two seeds. A distance map ϕ is first computed between the abdominal seed region $(I_F \vee E_1)$ which is fixed to maximum Φ_M and the background seed region I_M which is fixed to zero. The distance map encloses concave regions of $(I_F \vee E_1)$ by using $\frac{d\phi}{dt} = a\left(1 - H\left(\nabla^2\phi\right)\right)$, where t is the iteration, H is the Heavyside function, and $a > 1$. The Laplacian $\nabla^2\phi$ is computed within all 2D axial slices to give a distance ϕ over the entire 3D image.

The next step involves the graph cuts method that optimizes a Markov random field (MRF) formulation in 3D space over the smooth distance map ϕ with the same seed regions. The 26-connected neighborhood is used. The connection weights are computed from the difference of the values of ϕ between neighboring voxels. The weights are normalized with the inverse of the spatial distance to account for the anisotropic resolution. The application of the graph cuts method uses statistical priors from the distance map ϕ. The mean for the distribution of the abdomen is set to maximum Φ, Φ_M, and the mean for the distribution of the exterior region is set to $0.95 \times \Phi_M$. The standard deviation for both distributions is set to $\Phi_M/32$. The output provides the image region occupied by the entire abdomen I_{ABD}. The difference between I_{ABD} and the fat signal I_F gives the visceral background I_{BV}, $I_{ABD} - I_F = I_{BV}$. This region corresponds to organs in the abdominal region that do not normally contain fat such as the kidneys. The remaining background region $I_B - I_{BV}$ provides the background exterior to the body, I_{BO}, $I_B - I_{BV} = I_{BO}$ that is mainly air. The results of this processing step for the Dixon data shown in figure 2 are in figure 3.

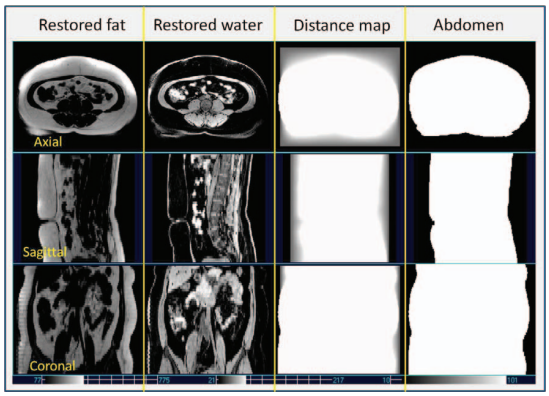


Fig. 3. The intensity restored fat and water images provide the abdominal body region.

2.4. Identification of the Visceral Abdominal Region

The next step is the segmentation of the outer boundary of the visceral region that is in contact with the subcutaneous fat. This is also performed with the graph cuts method [8]. The seeds for the visceral region is the visceral background I_{BV}. The visceral seeds in every slice are also extended with an ellipse as shape prior to give an elliptical cylinder E_2 with curved axis along the abdomen $(I_{BV} \vee E_2)$. The position and size of the ellipse is selected to ensure that the extended region always lies within the visceral region. Its mean position for the axial slice (c_x, c_y, z) has been computed in the previous section with the cumulative Radon projections. The size of the ellipse in I_{BV} is identical in every slice. The equation of the ellipse lying in the interior of the visceral region is $(x - c_x)^2/(1.8)^2 + (y - c_y)^2 < (5.7cm)^2$. The seed region for the subcutaneous fat is the outer background I_{BO}. This limits the domain over which the segmentation operates and thus decreases its time requirements. The segmentation is performed over the remaining ambiguous region between the two seed regions I_{BO} and $(I_{BV} \vee E_2)$. A potential field u is first computed based on the random walks algorithm, which is equivalent to the Laplace equation $\nabla^2 u = 0$ with fixed boundary conditions of $(I_{BV} \vee E_2)$ set to maximum potential and I_{BO} set to zero potential [9]. The field u is computed over the 3D image with 26-connected neighborhoods.

The graph cuts algorithm is then used that optimizes a MRF in 3D space over the potential field u. It is initialized with the same seed regions as the random walks step and does not make use of any statistical priors for u. The graph cuts operate in 3D with 26-connected neighborhoods. The connection weights are normalized with the inverse of the distance between neighboring voxels to account for the anisotropic resolution. The variation of the potential is low both within the subcutaneous and within the visceral fat regions, but is high at the boundary between the two regions. As a result the Graph cuts resolve the visceral region I_V from the subcutaneous fat region I_{FS}. The difference between I_V and I_{ABD}, gives the subcutaneous fat region I_{FS}, $I_{ABD} - I_V = I_{FS}$. The difference between I_{FS} and I_F provides the visceral fat image I_{FV}, $I_F - I_{FS} = I_{FV}$. The segmentation of the data shown in figure 2 and figure 3 is in figure 4.

3. RESULTS AND DISCUSSION

The method is implemented in C++ and the total average duration time of all the steps for the analysis of a dataset is approximately 6-7 hours on a multitasking Intel Xeon CPU of 2.27GHz. The same parameters have been used for all 32 datasets and for all steps of the analysis. Two additional segmentation examples are shown in figure 5. In figure 5 (a) for an obese subject and in figure 5 (b) for a thinner subject with a low quality image. The reasonable segmentation in figure 5 (b) demonstrates the robusness of the method. The joint

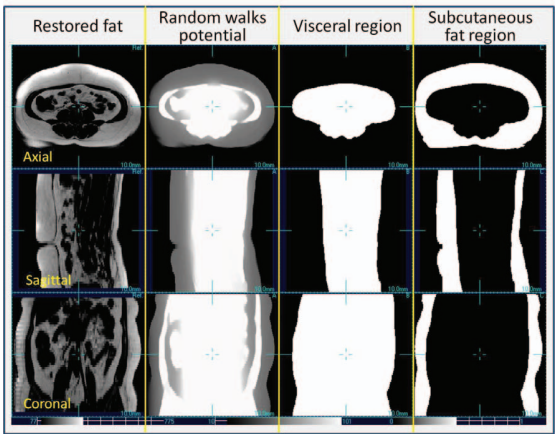


Fig. 4. The combination of the random walks and the graph cuts methods provide the interface between the visceral and the subcutaneous fat abdominal regions.

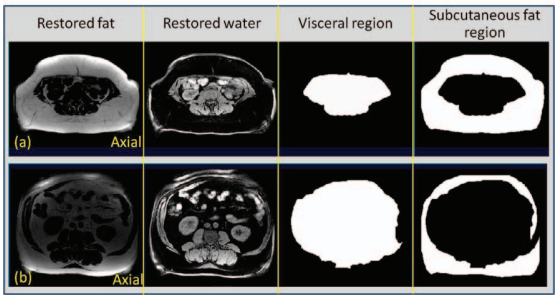


Fig. 5. Processing of data of an obese subject in (a) and of low quality data of a thinner subject in (b).

non-parametric intensity restoration can represent the variable fat occupancies and partial volume of the voxels in the visceral region effectively without assuming a finite number of parameterized classes [1]. The water image contributes to the restoration of the fat image, which is subsequently mainly processed. The random walks method [9] has been combined with the graph cuts method to improve the robustness of the segmentation to residuals of the intensity non-uniformity and other artifacts [9]. The method detects the entire internal fat, both the visceral fat as well as possibly the fat of the bone marrow of the vertebrae and the pelvis.

The visceral and subcutaneous abdominal regions have been successfully segmented from the 32 abdominal Dixon data sets. The segmentations of the relatively large abdominal images has been accelerated by limiting the analysis region to that expected to include the contours to be detected. The processing can also accomodate a variable topology in 3D. Thus, it is robust to noise or artifacts exterior to the body, it can represent possible folding of the subcutaneous fat in obese subjects, and can potentially be extended to other body regions. This is an improvement compared to 2D active contours represented as snakes that have been used extensively in this context and are limited to their initial topology [1]. This method is able to properly identify the visceral region and the internal fat by first resolving contacts between the visceral background and the exterior background and then resolving contacts between the visceral fat signal and the subcutaneous fat signal. The method is repeatable, general, and reliable.

4. REFERENCES

[1] V. Positano, T. Christiansen, M.F. Santarelli, S. Ringgaard, L. Landini, and A. Gastaldelli, "Accurate segmentation of subcutaneous and intermuscular adipose tissue from MR images of the thigh," *JMRI*, vol. 29, pp. 677–684, 2009.

[2] J. Kullberg, L. Johansson, H. Ahlstrom, F. Courivaud, P. Koken, H. Eggers, and P. Bornert, "Automated assessment of whole-body adipose tissue depots from continuously moving bed MRI: A feasibility study," *JMRI*, vol. 30, pp. 185–193, 2009.

[3] F. Klausmann, U. Ludwig, M. Honal, D. Koenig, P. Deibert, and S. Huff, "Accuracy of wholebody fat quantification with MRI: A comparison to air-displacement plethysmography," in *Proc. of ISMRM*, 2010.

[4] H. Mueller, F. Raudies, A. Unrath, H. Neumann, A.C. Ludolph, and J. Kassubek, "Quantification of human body fat tissue percentage by MRI," *NMR in biomedicine*, vol. 24, pp. 17–24, 2011.

[5] O.D. Leinhard, A. Johansson, J. Rydell, O. Smedby, F. Nystrom, P. Lundberg, and M. Borga, "Quantitative abdominal fat estimation using MRI," in *Proc. of ICPR*, 2008, pp. 1–4.

[6] Y. Jin, C.Z. Imielinska, A.F. Laine, J. Udupa, W. Shen, and S.B. Heymsfield, "Segmentation and evaluation of adipose tissue from whole body MRI scans," in *Proc. of MICCAI*, 2003, vol. 2878, pp. 635–642.

[7] S. Hadjidemetriou, M. Buechert, U. Ludwig, and J. Hennig, "Joint restoration of bi-contrast MRI data for spatial intensity non-uniformities," in *Proc. of IPMI*, 2011, pp. 346–358.

[8] Y. Boykov and G. Lea, "Graph cuts and efficient N-D image segmentation," *IJCV*, vol. 70, no. 2, pp. 109–131, 2006.

[9] L. Grady, "Random walks for image segmentation," *IEEE Trans. on PAMI*, vol. 28, no. 11, 2006.